50th AIAA Aerospace Sciences Meeting including the New Horizons Forum and Aerospace Exposition
09 - 12 January 2012, Nashville, Tennessee
AIAA 2012-0139

2D plasma flow in a magnetic nozzle with a bi-modal Electron Energy Distribution Function

M. Merino-Martínez*
Universidad Politécnica de Madrid, Spain

A two-dimensional plasma beam model is used to investigate the influence of a bi-modal Electron Energy Distribution Function, based on hot and cold electron populations, on the expansion of a current-free plasma through a divergent magnetic nozzle. Main results include the 2D plasma property profiles along the nozzle, for the complete quasineutral expansion regime; an analysis of quasineutral profile steepening and double layer formation in terms of the electron population parameters; the 2D structure of these flow features; and a study of their influence in the thrust, specific impulse, and plume efficiency provided by the nozzle.

I. Introduction

Magnetic nozzles constitute a promising accelerating device for electric space propulsion applications, and currently are one of the central elements in the development of advanced plasma thrusters, such as the *VAriable Specific Impulse Magnetoplasma Rocket* (VASIMR),[1] the *Applied-Field Magneto-Plasma-Dynamic Thruster* (AF-MPDT),[2,3] the *Helicon Thruster* (HT)[4,5,6] and the *Diverging Cusped field thruster* (DCFT).[7] They also present attractive benefits for a number of material processing and manufacturing applications.[8]

These nozzles consist in a convergent-divergent magnetic field, capable of guiding the plasma produced in the thruster chamber and accelerating it into vacuum. The plasma flow in a magnetic nozzle shows certain similarities with that of a heated neutral gas in a solid, *de Laval* nozzle,[9] as the plasma displays a sonic transition at the section of maximum magnetic field, B, and expands supersonically thereafter. Nevertheless, the key role of the electromagnetic interactions in a magnetic nozzle, the variety of acceleration mechanisms, and the involved plasma physics, give rise to new phenomena and complex flow characteristics, not present in the expansion of a neutral gas. Some of these phenomena can be benefited from for space propulsion applications, and can produce attractive gains in terms of the device performances.

The basic woking principle of these devices is based on the large mass difference between ions and electrons: while the former are heavier and fundamentally unaffected by moderated magnetic fields, the latter, much lighter, are completely magnetized, meaning that their trajectories are attached to the field and follow its geometry. Because of this, an appropriate magnetic field is able to radially confine the electron thermal expansion. As electrons describe the converging-diverging trajectory, an ambipolar electric field ensues in the plasma, which forces the (cold) ions to expand likewise. In this way, plasma internal (thermal) energy is converted to directed kinetic energy through the electric field.

The main advantages of magnetic nozzles over other accelerating devices are the ability to vary the produced thrust and specific impulse during operation, by altering the geometry and intensity of the applied magnetic field (the central idea behind the VASIMR, after which it is named), and the reduction/avoidance of plasma-wall contact due to the so-called magnetic screening effect, preventing serious temperature, heat transfer, efficiency decrease, and life reduction issues. Another key aspect is that, in order to neutralize the current-free beam, no external electrode is needed in principle, whose short life sets the limits of the durability of most space electric thrusters. Nevertheless, there are still some challenging aspects of magnetic nozzles which are not yet fully understood, such as the mechanisms of plasma detachment from the closed magnetic field lines far downstream, once the jet has been accelerated.

This article presents selected results from the MSc final project of the author, which has been carried out in the Polytechnic University of Madrid as part of the 'Helicon Plasma-Hydrazine combined micro'

*MSc Aerospace Engineer, mario.merino@upm.es

(HPH.com)[10] project of the 7th Framework Programme of the European Community[a]. The project HPH.com aims to produce a 50 W, dual-mode (hydrazine and plasma) thruster. In the plasma mode, it consists of a cylindrical helicon source where the plasma is produced and heated, and then, it expands and accelerates into the vacuum through a magnetic nozzle. Expected thruster performances are: 1.5 mN of thrust and a specific impulse $I_{sp} > 1200$ s.

The core aim of the MSc project is the formulation of a coherent physical model and simulation of the two-dimensional plasma expansion in a magnetic nozzle. A simulation code, baptized *DiMagNo* 2D,—acronym from 'Divergent Magnetic Nozzle,'—has been developed from zero in the project. This software implements and integrates the model numerically employing the Method of Characteristics (MoC), which makes it remarkably agile and precise, and the first of its type devoted to the simulation of magnetic nozzle flows.

Making use of the aforementioned model and code, this article presents the results of the investigation of the plasma expansion, flow phenomena and propulsive performances of a low-β, totally-ionized, collisionless plasma consisting of cold ions and hot electrons. It is shown that, under the right conditions, the inclusion of a small population of hotter electrons in the plasma, which results in a *bi-modal electron energy distribution function* (EEDF), causes the formation of certain plasma flow features known as quasineutral steepening layers (QSL) or current-free (CF) double layers (DL). This bi-modal EEDF, for the sake of simplicity, has been modeled as the superposition of two Maxwellian electron populations with distinct temperatures. The electric potential fall across these layers accelerates ions to high velocities in a short distance, which makes them an interesting phenomenon for space propulsion applications. The first set of results of the MSc Project, pertaining the plasma response and performances for a Maxwellian EEDF (a single electron species), has been recently presented.[11,12]

The rest of the paper is organized as follows: after briefly introducing the key ideas behind QSL and CF-DL formation, the role of non-Maxwellian EEDF, and commenting on some relevant experimental results in subsection A below, section II describes the full 2D model of the three-species plasma and the integration scheme, and characterizes the two-dimensional structure of the flow and its layer features in the nozzle. Next, section III highlights the main results regarding the device performances and plume efficiency, and the influence of the special EEDF on them. Finally, section IV summarizes the main conclusions of this work.

A. Plasma flow layer features and Non-Maxwellian EEDF

Essentially, a *quasineutral steepening layer* (QSL) is an electric potential fall of the order of the electron temperature, localized in a thin region of the flow, in which the plasma remains macroscopically quasineutral. When the thickness of this layer is of the order of some Debye lengths ($< 100\lambda_D$), plasma quasineutrality at the layer is not fulfilled, and one speaks of a double layer. A double layer consists of a positive and a negative Debye sheath, and connects two quasineutral regions of plasma. If no net electric current traverses the layer, it is called current-free (CF-DL). Because of its thinness in propulsive plasmas, the double layer is observed as a jump in the profiles of the electric potential and the plasma density.

Some of the most interesting phenomena appearing in magnetic nozzle flows, including QSL and CF-DL, are related to non-standard EEDF, such as when two coexisting electron populations of diverse temperature, one cold (c) and one hot (h), produce a bi-modal EEDF. This type of EEDF may be established during certain ionization and heating processes, such as those of helicon sources, where there is experimental evidence of the formation of energetic electron beams.[13]

The experiments of Hairapetian-Stenzel[14] prove the relation between the presence of hot electrons in an expanding collisionless plasma and a steepening of the electric potential profile, giving rise to a QSL, which under the right parameters becomes a CF-DL. The CF-DL is formed only in a limited range of temperature and density ratios of the two electron species.[15,16] Calling τ the hot-to-cold temperature ratio and α_0 the hot-to-total density ratio far upstream, a CF-DL forms for approximately $\tau > 10$ and a relatively low value of α_0.

Steepened but fully quasineutral QSL are formed for parametric values close to those leading to a double layer formation, which is also evidenced by their experiments. To this respect, it should be taken into account that distinction between a 'quasineutral region' and a 'non-neutral layer' has full sense only in the formal zero Debye length limit, i.e. $\lambda_D \ll L_c$, with L_c the other characteristic length of the problem.

[a]See http://www.hphcom.eu/

Charles and Boswell[4] have recently reported the formation of electric potential steepenings near the exit of a helicon source tube to a larger diffusion chamber, in the form of a CF-DL. Later, they detected ion beams with a large supersonic velocity (corresponding to a Mach number $M \simeq 2$),[17] which agrees with a potential jump in the double layer, about 3–4 times larger than the plasma temperature in the source. Due to all this evidence, the 'CF-DL helicon thruster' has been suggested as an innovative and attractive propulsion device.

When considering the energy equation of an ion in a collisionless plasma, $m_i u_i^2/2 + e\phi = \text{const}$, it is seen that whether the potential fall is more or less steepened, forming or not a double layer, is marginal for ion acceleration: as long as the plasma remains collisionless in the acceleration region, the ion beam kinetic energy is determined by the total fall of the electric potential. This fall depends on the hot electron temperature.[14] Nevertheless, it is desirable to accelerate ions in the shortest distance possible, since longer magnetic nozzles require stronger magnetic fields—and heavier field generators. Hence, ensuring that most of the potential fall will occur in a CF-DL or a QSL taking place in the near field of the nozzle is of interest for propulsive applications.

II. 2D Model formulation and numerical integration

The theoretical study of the plasma expansion in a magnetic nozzle requires establishing an appropriate model that captures all the physics of interest of the problem. The advantage of a two-dimensional model over a 1D one is the ability to recover the radial characteristics of the flow field, which among other benefits, allows to evaluate the plume efficiency of the nozzle—i.e., the divergence (or radial) losses of the jet. This section starts by formulating and describing the principal aspects of our 2D model. Unless indicated otherwise, the nomenclature used is conventional.

Consider a fully-ionized, collisionless, low-β plasma (defined as $\beta = 2\mu_0 p/B^2$, parameter that measures the relative importance of thermal pressure to magnetic pressure). Assume that the plasma is constituted of three species: cold (c) and hot (h) electron populations, and singly-charged cold ions (i). Further assume that this plasma is injected at ion-sonic velocity at the throat of an axisymmetric, diverging magnetic field, which will conform our magnetic nozzle. Under the hypothesis that the scale hierarchies

$$\lambda_D \ll \ell_e \ll R \ll \lambda_{col};\ m_e \ll m_i \tag{1}$$

are fulfilled—with ℓ_e the electron gyroradius, R the nozzle characteristic radius, and λ_{col} the shortest mean-free path of all collisional processes,—the evolution of the plasma can be adequately described with the following macroscopic, steady-state equations:

$$\nabla \cdot n_j \boldsymbol{u}_j = 0,\ (j = i, c, h)\,, \tag{2}$$

$$m_i n_i \boldsymbol{u}_i \cdot \nabla \boldsymbol{u}_i = -e n_i \nabla\phi + e n_i \boldsymbol{u}_i \wedge \boldsymbol{B}, \tag{3}$$

$$0 = -\nabla p_j + e n_j \nabla\phi - e n_j u_{\theta j} B \mathbf{1}_\perp = 0,\ (j = c, h)\,, \tag{4}$$

where $\mathbf{1}_\perp$ belongs to the orthonormal base $\{\boldsymbol{b} = \boldsymbol{B}/B, \mathbf{1}_\perp = \mathbf{1}_\theta \wedge \boldsymbol{b}, \mathbf{1}_\theta\}$, defined from the local magnetic field. Notice that, under these hypotheses, electron inertia and ion pressure have been neglected. From the length scale hierarchy of Eq. 1, it follows that electrons are completely magnetized—i.e., electron streamtubes (each species) coincide with magnetic streamtubes,—although ions can have any magnetization degree. As a consequence of the quasineutrality condition, implicitly expressed by $\lambda_D \ll R$, the last electron streamtube is also the last ion streamtube. Continuity equations (Eq. 2) show that a streamfunction ψ_j that verifies $\nabla\psi_j = n_j r \mathbf{1}_\theta \wedge \boldsymbol{u}_i$ exists for each species in the plasma ($j = i, c, h$). Similarly, there exists a magnetic streamfunction ψ_m satisfying $\nabla\psi_m = r\mathbf{1}_\theta \wedge \boldsymbol{B}$. As electron streamtubes are magnetic streamtubes, $\psi_j = \psi_j(\psi_m)$, for $j = c, h$.

Projecting Eq. 4 along $\boldsymbol{b}$ and modeling the electrons as two separate isothermal species provides

$$T_j \ln(n_j/n_{jS}) - e\phi = H_j(\psi_m)\,,\ (j = c, h) \tag{5}$$

where the subindex S denotes the throat section, $z = 0$, and n_{jS} is the particle density of species j at the origin. The function $H_j(\psi_m)$ is constant if the plasma is initially uniform. The same equation projected along $\mathbf{1}_\perp$ yields

$$e u_{\theta j}/r = -dH_e/d\psi_m, \tag{6}$$

which allows to calculate $u_{\theta j}$. From this expression it follows that, if $u_{\theta j}$ is initially zero in our non-collisional plasma, *it remains so throughout the expansion*. The ion momentum equation (Eq. 3) along $\mathbf{1}_\theta$ can be integrated to obtain

$$r m_i u_{\theta i} + e\psi = D_i\left(\psi_i\right), \tag{7}$$

which states the conservation of ion axial angular momentum. These relations conform a set of algebraic equations that provide n_c, n_h, and $u_{\theta j}$ $(j = i, c, h)$ as functions of ϕ, initial conditions, and the local value of the magnetic field.

Since ion flow is supersonic in the diverging nozzle, to obtain the variables u_{zi}, u_{ri} and ϕ, the method of characteristics (MoC) is employed to reduce the remaining partial differential equations—ion continuity equation, and ion momentum in the z and r directions—into ordinary differential equations along characteristic lines. The MoC exploits the physical properties of the problem, namely, that perturbations propagate along these curves. Due to this, the method is one of the fastest and most accurate for the solution of hyperbolic problems.[18]

The resulting equations along the Mach lines (denoted as the C_+, C_- curve families) and the ion streamlines (C_o) are:

$$u_{ri}\left.\frac{du_{zi}}{dz}\right|_{C_\pm} - u_{zi}\left.\frac{du_{ri}}{dz}\right|_{C_\pm} \mp \frac{e\sqrt{M^2-1}}{m_i}\left.\frac{d\phi}{dz}\right|_{C_\pm} = \\ = \left(u_{ri} - \lambda_\pm u_{zi}\right) f + \lambda_\pm g - h \tag{8}$$

$$\left.\frac{d}{dz}\right|_{C_o}\left(\frac{1}{2}m_i u_i^2 + e\phi\right) = 0 \tag{9}$$

where $\lambda_\pm = \left(u_{zi}u_{ri}/c_s^2 \pm \sqrt{M^2-1}\right)/\left(u_{zi}^2/c_s^2 - 1\right)$ and $\lambda_o = u_{ri}/u_{zi}$ are the local slopes of the characteristic curves, and

$$f = \sum_{j=c,h}\left(\frac{e n_j u_{\theta j}}{n T_j}\right)\left(u_{ri}B_z - u_{zi}B_r\right) - \frac{u_r}{r};$$

$$g = -u_{\theta i}\frac{eB_r}{m_i};\quad h = u_{\theta i}\frac{eB_z}{m_i} + \frac{u_{\theta i}^2}{r},$$

where c_s is the local ion sound velocity, $c_s = \sqrt{\gamma T/m_i}$, with γ the (effective) specific heat ratio defined as

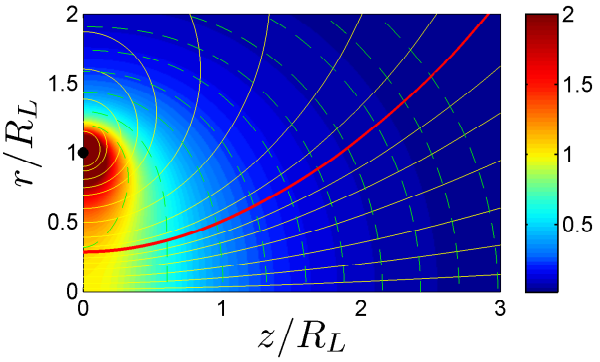

Figure 1: Meridian plane of the magnetic field created by a current loop placed at $r = R_L$. Yellow lines are field lines. The line chosen as nozzle outer line has been highlighted in red. Green, dashed lines represent B-constant lines. The background color shows the magnetic field intensity relative to B_S, its value at the origin.

$$\gamma = \frac{n}{p}\frac{dp}{dn} = \frac{n^2}{\left(n_h T_h + n_c T_c\right)\left(n_h/T_h + n_c/T_c\right)}, \tag{10}$$

and T the average electron temperature,

$$T = \left(n_h T_h + n_c T_c\right)/n. \tag{11}$$

Notice that Eq. 9 expresses the conservation of ion mechanical energy along streamlines, and that generally $H_i\left(\psi_i\right)$ can vary across streamlines, if initial conditions are not uniform.

Electron continuity equations then provide

$$\frac{n_j u_{\parallel j}}{B} = G_j\left(\psi_j\right),\ (j = c, h), \tag{12}$$

which, with a proper boundary condition, yield $u_{\parallel j}$, the component of the electron fluid velocity in the meridian plane (parallel to the magnetic field).

Although the model is applicable to any divergent magnetic nozzle, for the sake of illustration in the following the magnetic circuit is here reduced to a single current loop placed at $(z, r) = (0, R_L)$, with an intensity I_L flowing along 1_θ. For such a current loop, the magnetic streamfunction is:[19]

$$\psi_m\left(z, r\right) = \frac{2B_S R_L^2 r}{\pi}\cdot\frac{\left(2-k^2\right)\mathbf{K}\left(k^2\right) - 2\mathbf{E}\left(k^2\right)}{k^2\sqrt{\left(R_L + r\right)^2 + z^2}}, \tag{13}$$

where $k^2 = 4R_L r[(R_L + r)^2 + z^2]^{-1}$, $B_S = B_z(0,0) = \mu_0 I_L/(2R_L)$, and $\mathbf{K}(m)$ and $\mathbf{E}(m)$ are the complete elliptic integrals of the first and second kind.[20] The dimensionless number R_L/R_S, where R_S is the plasma radius at the throat, controls the divergence rate of the nozzle. The condition $\beta \ll 1$ implies that the magnetic field induced by the plasma internal currents can be neglected with respect to the applied field (at least, in the near-region of the nozzle). Hence, our nozzle's magnetic field geometry coincides with that of the guide field. Fig. 1 presents this magnetic field.

The mathematical expressions of the model can be made non-dimensional using n_S (total electron density at the origin), T_c, e, m_i, and R_S. Dimensionless variables will be distinguished with a hat, i.e., $\hat{u}_{zi} = u_{zi}/\sqrt{T_c/m_i}$ for the ion velocity, $\hat{\phi} = e\phi/T_c$ for the potential, and so on.

The model depends on the following non-dimensional parameters: $\tau = T_h/T_c$, the already introduced temperature ratio between the two electron species, and $\alpha_S = n_{hS}/n_S$, the hot-to-total density ratio at the origin. These two parameters are the object of our analysis. The problem also depends on R_L/R_S, which describes the divergence rate of the nozzle, and $\hat{\Omega}_{iS}$, the non-dimensional ion gyrofrequency at the origin, which evaluates the degree of ion magnetization. The values $\hat{R}_L = 3.5$ and $\hat{\Omega}_{iS} = 0.1$ were chosen as representative values of current thruster designs based on magnetic nozzles.[5,21] Also, nozzle performances improve for slowlier diverging fields and low ion magnetization, although plasma flow is almost uninfluenced by variations of the latter of these parameters in the range 0.01–10.[12]

The dependency of $\hat{n}$, $\hat{T}$, $\hat{c}_s$ and γ on $\hat{\phi}$ is illustrated in Fig. 2, which portraits the anomalous thermodynamics of the plasma, caused by the bi-modal EEDF. The most outstanding feature is the unusual behavior of the specific heat ratio, γ, whose value $\gamma < 1$ means that the average electron temperature T increases as the plasma travels downstream. This is due to the fact that cold electrons are effectively confined by the electric potential fall that occurs as the plasma expands, while hotter, more energetic electrons are able to travel further downstream. As it will be seen, this effect is responsible of the formation of special layer features in the flow.

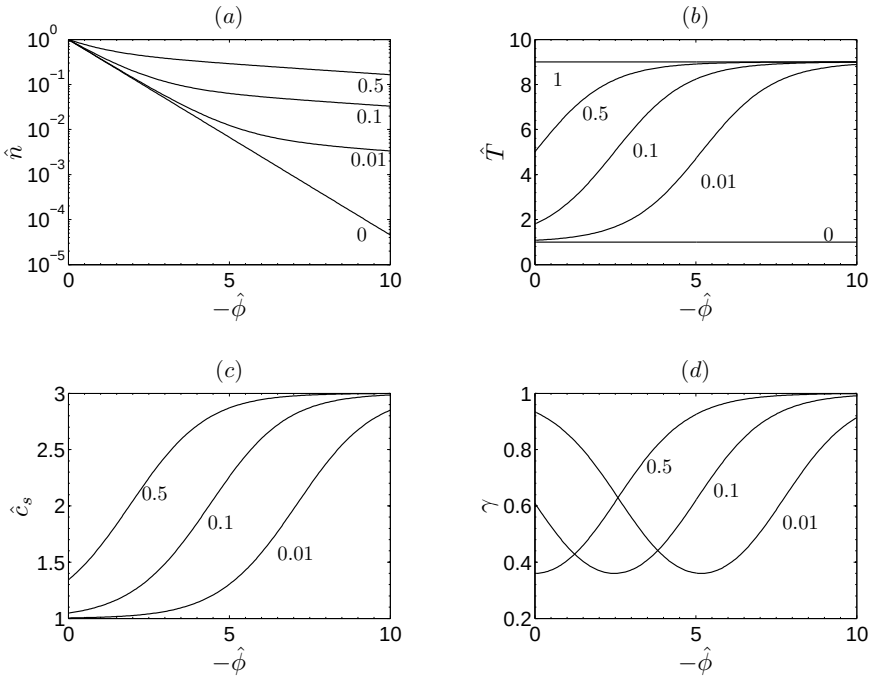

Figure 2: Dependence of the main variables with ϕ for $\tau = 9$. Numbers by the lines indicate the value of α_S of each line.

In regard to the initial conditions at the throat, for this analysis we will choose a uniform plasma with no electrical currents, entering the nozzle at a velocity slightly higher than the sonic velocity, to make the problem completely hyperbolic in order to apply the MoC (a ion Mach number $M_S = 1.05$ was chosen, after checking that the solution was insensitive to small variations of M_S when $M_S - 1 \ll 1$).

Previous work by Ahedo and Martínez-Sánchez[15,16] using a 1D model point out the existence of different

parametric regions where a CF-DL forms in the convergent side, throat or divergent side of the nozzle. Fig. 3 presents the region of the τ, α_S plane where a CF-DL forms in the divergent nozzle, which is delimited by a curve. In the following, we will perform our 2D analysis by studying the plasma response as we increase α_S and approach $\alpha_{S,1}$ for different values of τ.

Fig. 4 covers a number of cases with $\tau = 9$. In these graphs, the different variables have been referred to T_S,

$$T_S = (1 - \alpha_S)\, T_c + \alpha_S T_h, \tag{14}$$

which allows to compare the behavior of each plasma in equal terms with respect to their internal energy at the throat. This shows an interesting increase in the total potential fall for the three-species plasma, when compared against a single electron species plasma, between sections S and the chosen exit section at $\hat{z} = 6$, E (which has an exit radius of $\hat{R}_E = 3.15$, and hence the nozzle's area ratio is roughly $\varepsilon \simeq 10$).

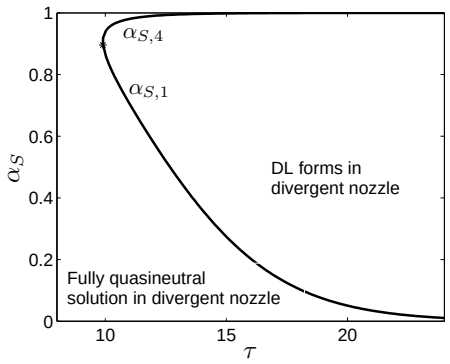

Figure 3: Parametric regions of the plane τ, α_S, portraying a quasineutral expansion region and a zone where CF-DL form. The curve given by the functions $\alpha_S(\tau) = \alpha_{S,1}$ and $\alpha_{S,4}$ separate both regions. (Adapted here from the 1D model analysis of Ahedo and Martínez-Sánchez[16]).

As it can be seen, a mild QSL forms at different positions in the nozzle, and it moves toward the throat as α_S increases. The Mach number decreases and reaches a minimum around this spot. This outstanding behavior is a result of the specific heat ratio being lower than 1, as seen in fig. 2, which makes the average plasma temperature and the sonic velocity c_s to increase, while the ion Mach number decreases. This is an effect of the anomalous thermodynamics, and causes a large electric potential fall to concentrate in this region, giving rise to the QSL. The 2D expansion points out that the minimum Mach number is reached first on the plasma edge than on the axis. Actual ion velocity is always monotonic, and increases substantially with respect to the reference case, due to the increased electric potential fall produced by the presence of hot electrons. This velocity presents large differences between its value on the outer and inner lines, specially around the QSL. This difference decreases after this steepening, to start increasing slowly afterward again. The fact that $u_i/\sqrt{T_S/m_i}$ is larger in the simulation with $\alpha_S = 0.2$ (blue) than in the one with $\alpha_S = 0.1$ (red) in spite of the nearly equal final potential $\hat{\phi}$ is due to the role of the specific heat ratio function: from the equation of ion energy, Eq. 9: $u_i^2/(T_S/m_i) = 1 - 2e\phi/(T_S\gamma)$.

Fig. 4 (c) shows that downstream of the QSL, the potential at the exterior line falls at a higher rate than at the center line. This difference of potential translates into a radial electric field that accelerates ions, adding to the radial losses. The QSL has a maximum E_z electric field on the axis, fig. 4 (d), at roughly $\alpha_S = 55\%$ when measured relative to T_c, and at low α_S relative to T_S. However, this larger maximum of the electric field for low α_S takes place always further downstream as α_S is decreased, revealing the necessity to operate with ever larger magnetic nozzles—and therefore ever stronger magnetic fields—to take advantage of this flow phenomenon. Therefore, for propulsion applications, where the objective is to deliver maximal thrust at minimum weight, it may be interesting to position the QSL closer to the nozzle throat, so ions are earlier accelerated by this structure.

Analogously, Fig. 5 presents the results for $\tau = 18$. In this case, as we are approaching the limit line $\alpha_{S,1}(\tau)$, the Mach number at the steepening point decreases rapidly to 1, again due to the anomalous behavior of γ. The simulation with $\alpha_S = 0.09$ presents a very sharp minimum of M on both the outer and center streamlines, which for $\alpha_{S,1}$ would actually become an angulous point, revealing the onset of a CF-DL discontinuity, and at the same time the flow would become (sub)sonic. On this line and beyond, the existence of a secondary sonic transition turns the system of equations parabolic at that position, and the integration with the MoC is stopped. At any rate, the cases of propulsive interest are those where the hot-to-total electron density ratio is small, say $\alpha_S < 0.1$, and we will focus our analysis on them. Ion velocity differences between both streamlines in the neighborhood of the QSL become much larger for $\tau = 18$ than for $\tau = 9$. Interestingly, the potential along these streamlines does not diverge as much as for $\tau = 9$ after the steepening. The maximum electric field on the axis is very acute, and would become infinite when the CF-DL discontinuity develops, at $\alpha_{S,1}$.

As it can be seen in Figs. 4 and 5, the evolution of the plasma along the axis line and the outer streamline

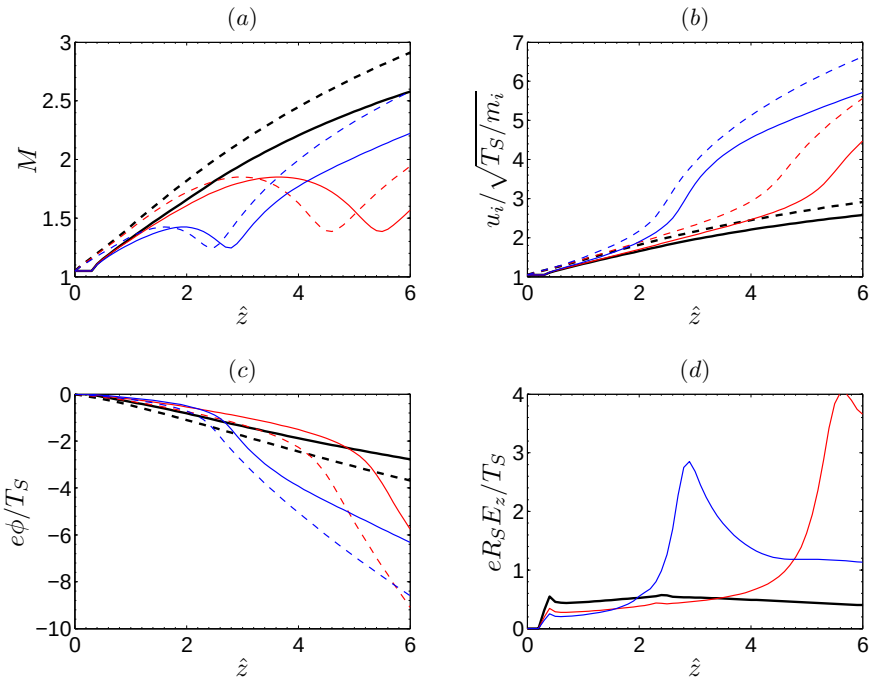

Figure 4: 2D plasma expansion profiles with $\tau = 9$. Various simulations with different α_S have been plotted: thick lines represent the reference two-species plasma ($\alpha_S = 0$ or $\alpha_S = 1$, which coincide since results are referred to T_S). Red lines show $\alpha_S = 0.1$, and blue lines $\alpha_S = 0.2$. Values at the center line are in solid lines. Dashed lines refer to the exterior streamline. End section, $\hat{z}_E = 6$, has $\hat{R}_E \simeq 3.15$.

is similar for each variable, but the position of the QSL on the outer one occurs slightly before than on the center one. This reveals the 2D structure of this flow feature, which can be better appreciated in Fig. 6. While potential isolines possess a near-parabolic shape, with a curvature that increases further downstream (note however that in the $\tau = 18$ case this shape becomes slightly more complicated downstream of the QSL), the geometry of the region of maximum electric field, eR_SE/T_S, does not exactly coincide with these lines, and presents a slightly different shape. This is due to the fact that ϕ-isolines are less spaced at the outer streamline than at the axis, because of their increasing curvature. This shows that radial differences exist that affect the way ions are accelerated, and additionally indicates that it is preferable to have the QSL close to the throat, as it becomes more planar and most ion acceleration across it would be in the z-direction, reducing radial losses.

III. Propulsive performances of the three-species plasma

After characterizing the plasma expansion in the quasineutral parametric region with the 2D model, we now turn our attention to the influence of the hot electron tail on the propulsive parameters of the nozzle. Although our plasma model can estimate the propulsive gains and the radial losses, it cannot provide information on the global efficiencies of the device. This would require matching with (a) the upstream process of plasma ionization and heating, and (b) the modeling of the magnetic detachment far downstream, which is out of the scope of the present work.

The main parameters of interest that describe the potential of the system as an accelerating device are the produced thrust F_E, the specific impulse $I_{sp} = F_E/\dot{m}_i$ (here in velocity units), and the plume efficiency η_{plume}. Since I_{sp} is the effective plasma velocity at the nozzle exhaust, its increment with respect to ion velocity at the entrance is approximately proportional to the square root of the total potential fall between stations S and E: $I_{sp} \propto \sqrt{2e\left(\phi_S - \phi_E\right)/m_i}$. A first measure of the energy spent on the plasma in the thruster chamber is the average electron temperature at the origin, T_S. Therefore, for propulsion applications it is of great interest to analyze the potential fall obtained for different τ, α_S, relative to this

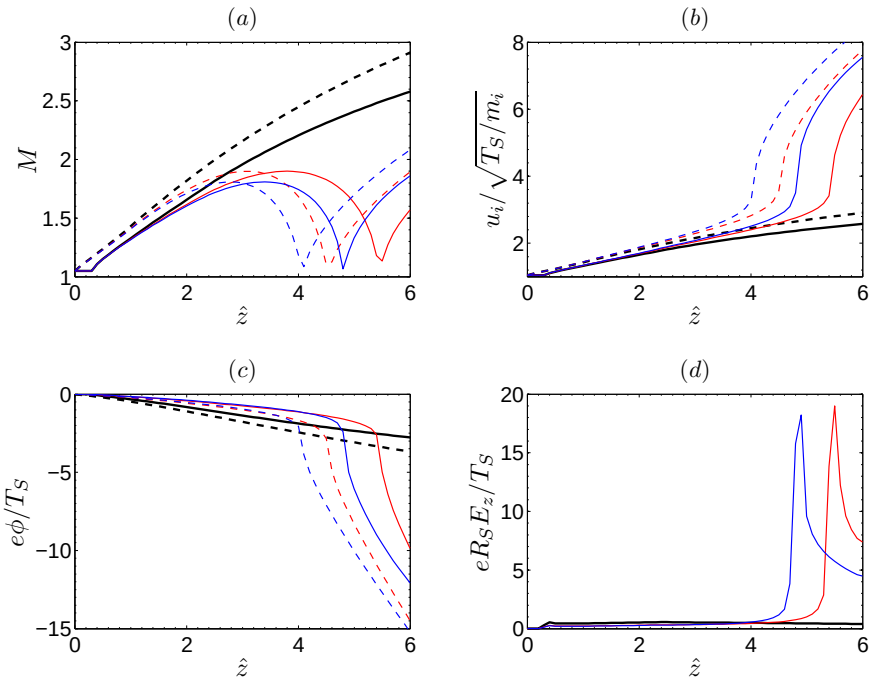

Figure 5: 2D plasma expansion profiles with $\tau = 18$. Similarly to the previous figure, thick lines are for the reference, two-species plasma ($\alpha_S = 0$ or $\alpha_S = 1$). Red lines show $\alpha_S = 0.07$, and blue lines $\alpha_S = 0.09$, very close to the limit line $\alpha_{S,1}(\tau)$ of CFDL formation. Values at the center line are in solid lines. Dashed lines refer to the exterior streamline. Again end section is located at $\hat{z}_E = 6$, with $R_E \simeq 3.15$.

temperature. This fall was shown in Figs. 4 and 5. As it can be seen, a small fraction of hot electrons ($\alpha_S \simeq 0.1$) can more than triple the normalized potential fall along the nozzle. This outstanding result claims that three-species plasmas can bring important benefits, in terms of higher propulsive performances. A minor decrease in potential fall is registered for α_S too small. This is due to the QSL taking place after section E, which would otherwise increase this fall as for higher α_S.

The plasma total momentum flux along the nozzle at $z = \text{const}$ sections, $F(z)$, can be separated into its ion/momentum and electron/pressure contributions, i.e.,

$$F(z) = F_i(z) + F_e(z), \tag{15}$$

with

$$F_i = \int_{A(z)} m_i n u_i^2 dA,\; F_e = \int_{A(z)} (n_c T_c + n_h T_h) dA. \tag{16}$$

As the magnetic nozzle transforms internal plasma energy into kinetic energy, ion/momentum thrust increases while electron/pressure thrust decreases. Fig. 7 depicts this thrust development, comparing a two-species plasma with diverse three-species ones. As it can be seen, the hot electron tail causes a large increase in ion/momentum thrust at the location of the QSL, becoming more than two times larger in certain cases. The total plasma momentum also increases with respect to the reference, two-species plasma, although this increase is not concentrated at any particular position. The differences between the profiles of the total momentum for different values of α_S are smaller than for the ion momentum. This is due to the electron/pressure contribution to the total momentum, which registers a large fall at the QSL position, compensating for the increase in ion/momentum thrust.

The ratio of thrust between stations S and E is defined as F_E/F_S, which coincides with the ratio of the specific impulse to $F_S/\dot{m}_i$ — i.e., the specific impulse that would be obtained if no nozzle existed. These two factors are independent of the plasma internal energy at the throat, but depend largely on the electron population parameters τ, α_S.

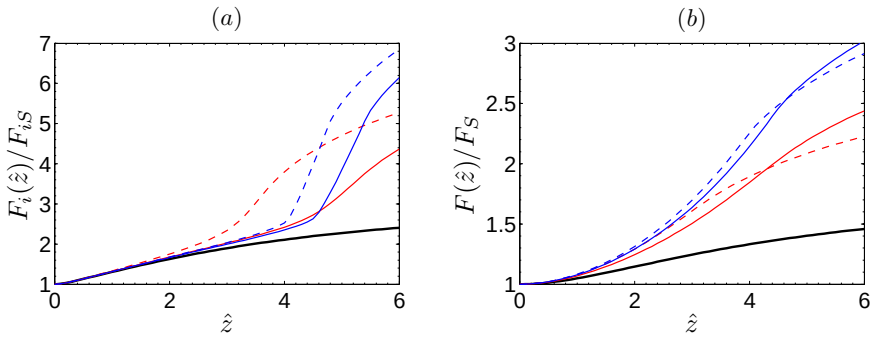

Figure 7: Ion and total plasma momentum evolution along the nozzle at $z = \text{const}$ sections. Thick black lines are the reference two-species plasma. Red lines denote $\tau = 9$ (with $\alpha_S = 0.1$ for the solid line, and $\alpha_S = 0.2$ for the dashed line). Blue lines indicate $\tau = 18$ (with $\alpha_S = 0.07$ for the solid line, and $\alpha_S = 0.09$ for the dashed line).

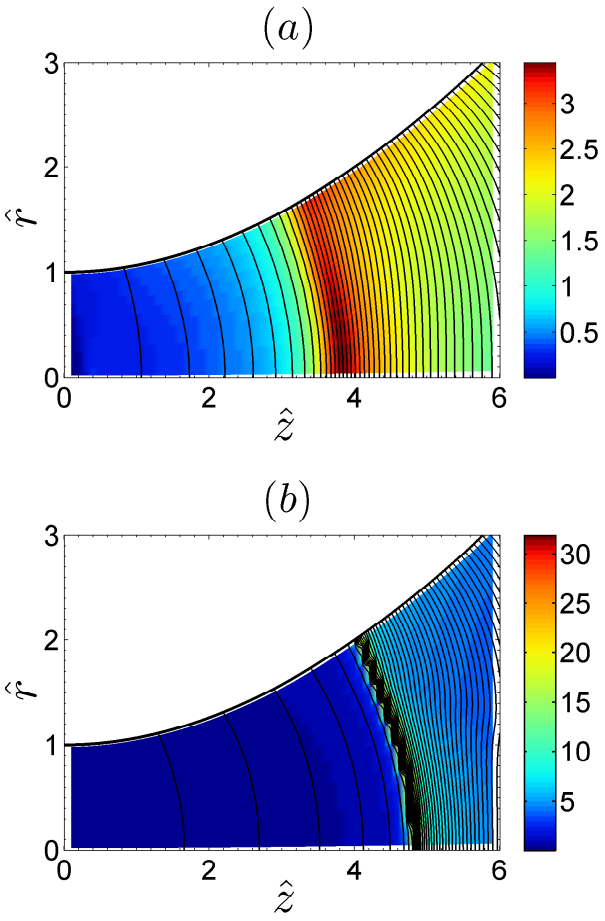

Figure 6: Electric field intensity inside the nozzle, eR_SE/T_S (background color), and plasma potential isolines. Figure (a) shows a mild QSL, for $\tau = 9$ and $\alpha_S = 0.2$. Figure (b) presents a much more intense QSL, for $\tau = 18$ and $\alpha_S = 0.09$.

The nozzle (or plume) efficiency η_{plume} reflects the amount of kinetic energy that is wasted in radial losses, and it is one of the factors contributing to thrust efficiency of the whole thruster. Defined at each $z = \text{const}$ section, its expression is:

$$\eta_{plume}(z) = \frac{P_{zi}(z)}{P_i(z)} \simeq \frac{F_i^2(z)}{2\dot{m}_i P_i(z)} \tag{17}$$

with the axial and total ion kinetic powers defined as

$$P_{zi}(z) = \int_{A(z)} \frac{1}{2} m_i n u_{zi}^3 dA,$$
$$P_i(z) = \int_{A(z)} \frac{1}{2} m_i n u_i^2 u_{zi} dA. \tag{18}$$

Simulation results presented in Fig. 8 point out that no relevant change in plume efficiency occurs. However, a slight decrease in η_{plume} with respect to the two-species plasma case is found locally around the QSL, which is afterward recovered. In some cases ($\tau = 18$, for instance), η_{plume} reaches a minimum, after which it increases again in a small region. This apparently surprising result can be explained if we consider the 2D structure of the plasma expansion: as we saw in Fig. 6, the QSL takes place along a slightly curved line, and not at $z = \text{const}$. When ions cross this line, they experience a large acceleration, and due to its curved shape, ions near the outer border are accelerated first, and acquire a strong radial component. This affects the overall efficiency at that $z = \text{const}$ section, lowering it. Some distance downstream, centerline ions cross the QSL, gaining a large axial velocity, which compensates for this decrease, and (temporarily) rises the value of η_{plume} again.

To separate the influence of the 2D geometry of the problem at hand, we shall also define the plume

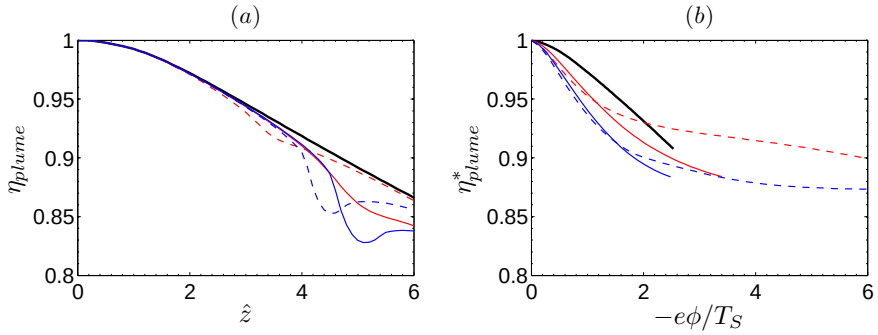

Figure 8: Plume efficiency obtained with the magnetic nozzle for different plasmas. Figure (a) presents this value on z-constant surfaces. Figure (b) displays the value of η_{plume} on ϕ-constant surfaces, denoted by η^*_{plume}. Thick black lines show the reference, two-species plasma case. Red lines correspond to $\tau = 9$ (solid: $\alpha_S = 0.1$, dashed: $\alpha_S = 0.2$), and blue lines to $\tau = 18$ (solid: $\alpha_S = 0.07$, dashed: $\alpha_S = 0.09$).

efficiency at ϕ-constant surfaces, η^*_{plume}:

$$\eta^*_{plume}(\phi) = \frac{P^*_{zi}(\phi)}{P^*_i(\phi)}, \tag{19}$$

where

$$P^*_{zi}(\phi) = \int_{A(\phi)} \frac{1}{2} m_i n u_{zi}^2 \boldsymbol{u}_i \cdot \boldsymbol{n} dA,$$
$$P^*_i(\phi) = \int_{A(\phi)} \frac{1}{2} m_i n u_i^2 \boldsymbol{u}_i \cdot \boldsymbol{n} dA. \tag{20}$$

The graph of Fig. 8 (b) presents the value of η^*_{plume} at constant-$(e\phi/T_S)$ surfaces. As it can be seen, now the efficiency decreases monotonically. Notice that, since each simulation reaches a different final value of the potential, ϕ_E, each line ends at a different abscissa. From this figure, some conclusions can be drawn about the actual behavior of the plume efficiency in terms of τ and α_S. First of all, the presence of a hot electron tail causes a minor negative effect on the efficiency, slightly increasing radial losses. This effect seems to be more pronounced for higher τ. With respect to the influence of α_S, η^*_{plume} is maximal for $\alpha_S = 0$ (two-species plasma). As α_S increases from 0, this efficiency starts to decrease and soon reaches a minimum. For higher values of α_S, the efficiency slowly increases again, since lines for $\alpha_S = 1$ and $\alpha_S = 0$ coincide.

IV. Conclusions

This paper has analyzed the influence of a bi-modal electron energy distribution function (modeled as two coexisting hot and cold electron populations) on the plasma expansion through a divergent magnetic nozzle. A 2D model has been used to characterize the three-species plasma flow, and discuss the appearance of quasineutral steepening layers in the plasma magnitudes. These special flow features can coalesce into non-neutral current-free double layers, depending on the value of the electron species parameters that define the EEDF: the electron temperature ratio τ, density ratio at the throat α_S. Results reveal that a small hot electron tail can induce vast benefits on the propulsive performances of the magnetic nozzle. The relative thrust and specific impulse can more than double if the temperature and density ratios are adequate. Although the plume efficiency, η_{plume}, suffers a minor decrease, it is nevertheless outweighed by the largely increased total potential fall that the three-species plasma cause. Simulations reveal the curved shape of the ϕ-constant lines, and that the maximal E field line does not coincide with them.

Additionally, all the analyses lead us to conclude that the gains are due to the increased potential fall caused by the anomalous thermodynamics—characterized by an effective specific heat ratio γ lower than 1, meaning that the plasma temperature rises as it expands. The magnitude of this fall depends strongly on the temperature ratio τ. Whether this fall occurs in a quasineutral steepening layer or a double layer is irrelevant for the plasma response, as long as it takes place in the near plasma field. Actually, the difference

between both is a matter of scale only. The double layer formation has no role in the propulsion gain, it is only another consequence of these thermodynamics.

During this project a fast and accurate software called DiMagNo 2D has been developed for the investigation of magnetic nozzles, which employs the method of characteristics to calculate the flow field in the diverging nozzle. Due to its modularity, it allows to study magnetized plasma flows under many different conditions. Our current research is focused on the problem of plasma detachment from the magnetic nozzle, for which the DiMagNo code has proven to be a valuable tool.

Acknowledgments

The author would like to express his gratitude to E. Ahedo for our long, mind-opening discussions, and his invaluable support and dedication as the supervisor of this MSc project.

This work was financed by Gobierno de España (Plan Nacional de I+D, Project ESP2007-62694) and the European Community (7th Framework Programme, Grant 218862, project HPH.com).

References

[1]Arefiev, A. and Breizman, B., "Theoretical components of the VASIMR plasma propulsion concept," *Physics of Plasmas*, Vol. 11, No. 5, 2004, pp. 2942–2949.

[2]Sasoh, A. and Arakawa, Y., "Electromagnetic effects in an applied-field magnetoplasmadynamic thruster," *Journal of Propulsion and Power*, Vol. 8, No. 1, 1992, pp. 98–102.

[3]Krülle, G., Auweter-Kurtz, M., and Sasoh, A., "Technology and application aspects of applied field magnetoplasmadynamic propulsion," *J. Propulsion and Power*, Vol. 14, 1998, pp. 754–763.

[4]Charles, C. and Boswell, R., "Current-free double-layer formation in a high-density helicon discharge," *Applied Physics Letters*, Vol. 82, No. 9, 2003, pp. 1356–1358.

[5]Batishchev, O., "Minihelicon Plasma Thruster," *IEEE Transaction on Plasma Science*, Vol. 37, 2009, pp. 1563–1571.

[6]Ziemba, T., Carscadden, J., Slough, J., Prager, J., and Winglee, R., "High Power Helicon Thruster," *41th Joint Propulsion Conference, Tucson, AR*, AIAA 2005-4119, American Institute of Aeronautics and Astronautics, Washington DC, 2005.

[7]Courtney, D. and Martinez-Sanchez, M., "Diverging Cusped-Field Hall Thruster," *30th International Electric Propulsion Conference, Florence, Italy*, IEPC-2007-39, Electric Rocket Propulsion Society, Fairview Park, OH, 2007.

[8]Schoenberg, K., Gerwin, R., Moses, R., Scheuer, J., and Wagner, H., "Magnetohydrodynamic flow physics of magnetically nozzled plasma accelerators with applications to advanced manufacturing," *Physics of Plasmas*, Vol. 5, 1998, pp. 2090–2104.

[9]Andersen, S. A., Jensen, V. O., Nielsen, P., and D'Angelo, N., "Continuous Supersonic Plasma Wind Tunnel," *Phys. Fluids*, Vol. 12, 1969, pp. 557–560.

[10]Ferri, D. P. F., Manente, M., Curreli, D., Guclu, Y., Melazzi, D., Rondini, D., Suman, S., Carlsson, J., Bramanti, C., Ahedo, E., Lancellotti, V., K.Katsonis, and Markelov, G., "Design of 50W Helicon Plasma Thruster," *31th International Electric Propulsion Conference, Ann Arbor, Michigan, USA*, IEPC 2009-205, Electric Rocket Propulsion Society, Fairview Park, OH, 2009.

[11]Ahedo, E. and Merino, M., "Two-dimensional plasma acceleration in a divergent magnetic nozzle," *44th Joint Propulsion Conference, Hartford, CT*, AIAA 2009-5361, American Institute of Aeronautics and Astronautics, Washington DC, 2008.

[12]Ahedo, E. and Merino, M., "Two-dimensional supersonic plasma acceleration in a magnetic nozzle," *Physics of Plasmas*, Vol. 17, 2010, pp. 073501.

[13]Chen, R. T. S. and Hershkowitz, N., "Multiple Electron Beams Generated by a Helicon Plasma Discharge," *Physical Review Letters*, Vol. 80, 1998, pp. 4677–4680.

[14]Hairapetian, G. and Stenzel, R. L., "Particle dynamics and current-free double layers in an expanding, collisionless, two-electron-population plasma," *Physics of Fluids B*, Vol. 3, No. 4, 1991, pp. 899–914.

[15]Ahedo, E. and Martinez-Sanchez, M., "The Role Of Current-Free Double-Layers In Plasma Propulsion," *44th Joint Propulsion Conference, Hartford, CT*, AIAA 2008-5005, American Institute of Aeronautics and Astronautics, Washington DC, 2008.

[16]Ahedo, E. and Martinez-Sanchez, M., "Theory of a stationary current-free double-layer in a collisionless plasma," *Physical Review Letters*, Vol. 103, 2009, pp. 135002.

[17]Charles, C. and Boswell, R., "Laboratory evidence of a supersonic ion beam generated by a current-free 'helicon' double-layer," *Physics of Plasmas*, Vol. 11, 2004, pp. 1706–1714.

[18]Zucrow, M. and Hoffman, J., *Gas dynamics* , Wiley, New York, 1976.

[19]Jackson, J., *Classical Electrodynamics*, Wiley, New York, 1999.

[20]Abramowitz, M. and Stegun, I., *Handbook of Mathematical Functions*, Dover, New York, 1965.

[21]Winglee, R., Ziemba, T., Giersch, L., Prager, J., Carscadden, J., and Roberson, B. R., "Simulation and laboratory validation of magnetic nozzle effects for the high power helicon thruster," *Physics of Plasmas*, Vol. 14, 2007, pp. 063501.